SCIENTIFIC AND TECHNICAL SECTION

UDC 539.4

Numerical Simulation of the Inlet/Outlet Pressure Ratio Effect on the Heat Transfer Coefficient in an Air Turbine Cascade

Z. He, J. H. Lin, X. Y. Sun,[1] and X. Gu

College of Aerospace and Civil Engineering, Harbin Engineering University, Harbin, China

[1] sunxiaoyu520634@163.com

Based on the state-of-the art methods of gas turbine cascade heat transfer assessment, a theoretical model of the two-dimensional air turbine cascade is proposed, wherein gas flows past the turbine blade profile. The velocity, temperature, and pressure fields, as well as the heat transfer distribution along the pressure and suction surfaces, the leading and trailing edges of the turbine blade were computed via FLUENT software at different pressure ratios. This permitted of studying the heat transfer evolution at different pressure ratios in the same position and at the same pressure ratio in different positions.

Keywords: pressure ratio, heat transfer, turbine cascade.

Introduction. Heat transfer cooling analysis is crucial for design of aero-engine turbine blades and very topical in aerodynamic research of aircraft [1]. Since heat transfer in a turbine cascade channel with gas flow is quite complex, its cooling design necessitates a convenient and accurate assessment of the heat transfer characteristics of the turbine working surface, e.g., using an effective numerical simulation method, which would provide a quick and accurate calculation of the heat transfer coefficient. In this paper, the pressure ratio effect on the heat transfer coefficient in the turbine cascade is explored via such simulation.

Since 1970s, the film cooling technology became a hotspot research subject of domestic and foreign scholars [2]. On the one hand, numerous studies were focused on the mechanism of flat film cooling, which involved flow parameters (Reynolds number, blowing ratio, momentum ratio, pressure gradient, turbulence, density ratio, etc.) and geometrical parameters (film hole shape, diameter, hole spacing, etc.) affecting the heat transfer coefficient and cooling efficiency [3, 4]. On the other hand, some studies investigated the application of the turbine blade film holes under the test conditions, to assess the surface heat transfer coefficient and the film cooling efficiency for blades with film holes under the working conditions, for the further prediction of the blade surface temperature, blade strength and durability [5].

Thus, Nealy et al. [6] revealed the basic factors controlling the surface heat transfer of the blade, which included boundary layer transition characteristics, free flow turbulence, pressure gradient, cooling working material injection position, blade surface curvature, blade surface roughness, airflow separation and reattachment, and shock wave/boundary layer interaction. An attempt to account for the effect of these factors on the heat transfer was made by these researchers with the emphasis on the Mach and Reynolds numbers.

Alternatively, a group of researchers from the Institute of Engineering Thermophysics of the Chinese Academy of Sciences (Beijing, China) [7] have studied the distribution of cooling efficiency across the single-row circular orifice of 30°, single row of diagonal holes and downstream of the single-row square holes by the heat and mass transfer mass method. They have inducted the cooling efficiency empirical formula in the middle line position of a certain area downstream of the nozzle by the least squares method. The results show that the cooling efficiency is very high.

Liu et al. [8] proposed the thermal conductance of graphene–matrix interfaces plays a key role in controlling the thermal properties of graphene-based nanocomposites. It represents if heat enters graphene from its basal plane one side and then leaves it the other side at once, the corresponding interfacial thermal conductance is large; if heat enters graphene from both sides of its basal plane and leaves it at a position on its basal plane at a moment, the corresponding interfacial thermal conductance is small.

Cao et al. [9] proposed an article of probing nanoscale thermal transport in surfactant solutions in 2015. They examined the thermal transport and structure in solution of AOT in n-octane liquids using small-angle neutron scattering, thermal conductivity measurements, the result shows that: the thermal conductivity of the surfactant solution decreases as AOT is added until the onset of micellization but increases as more AOT is added.

1. **Theoretical Solutions and Their Software Implementation**. The flow process related to heat transfer problem addressed in this paper can be reduced to the Navier–Stokes equations in the following form:

$$\frac{\partial}{\partial x_i}(\rho u_i) = 0, \tag{1}$$

$$\frac{\partial}{\partial x_j}(\rho u_i u_j) = -\frac{\partial p}{\partial x_i} + \frac{\partial}{\partial x_j}\left[\mu\left(\frac{\partial u_i}{\partial x_j} + \frac{\partial u_j}{\partial x_i}\right)\right] + \frac{\partial}{\partial x_j}(-\rho\overline{u_i' u_j'}), \tag{2}$$

$$\frac{\partial}{\partial x_i}(\rho u_i c_p T) = \frac{\partial}{\partial x_i}\left[\alpha_T\left(\mu_{eff}\frac{\partial T}{\partial x_i}\right)\right] + \frac{\partial u_i}{\partial x_j}\left[\mu_{eff}\left(\frac{\partial u_i}{\partial x_j} + \frac{\partial u_j}{\partial x_i}\right) - \frac{2}{3}\mu_{eff}\frac{\partial u_k}{\partial x_k}\right]. \tag{3}$$

From the fluid mechanics, the set of Navier–Stokes equations (which contain a mass conservation equation and three momentum conservation equations) allows one to derive four physical parameters. The system of Navier–Stokes equations has a closed form and, thus, can yield accurate theoretical solutions. However, since their derivation requires significant computational resources of direct numerical simulation (DNS), such solutions are not widely used by the engineers. For engineering applications, alternative two-equation eddy-viscosity turbulence models were proposed by Menter in 1994 [10]. These included k-epsilon(ε) equation turbulence model for the near-wall region and k-omega(ω) equation turbulence model for the far field, where k is turbulent kinetic energy, ω is specific dissipation, which determines the turbulence scale, and ε is turbulent dissipation.

Based on this model, FLUENT software package was developed for simulating and analyzing complex flow field areas. It is mainly applied to fluid flow and heat transfer in the flow field. It supports a variety grid of different formats applicable to ICEM, GAMBIT, and mechanical CAD software products relevant to a wide range of applications in the automotive, aviation, aerospace, turbine, oil and gas industries. Moreover, FLUENT can accurately simulate the non-viscous flow, laminar flow, and turbulence. Therefore, in this study, the FLUENT software package was used for the implementation of shear stress

transport (SST) $k-\omega$ turbulence model, which combines the advantages of the $k-\varepsilon$ equation turbulence model and the $k-\omega$ turbulence model. The former model is automatically substituted by the latter one, depending on the distance from the wall. The convergence condition is less than 10^{-6} for the parameter residual, while k and ε equations are shown as follows:

$$\frac{\partial}{\partial x_i}(\rho u_i k)=\frac{\partial}{\partial x_i}\left[\left(\mu+\frac{\mu_t}{\sigma_\varepsilon}\right)\frac{\partial k}{\partial x_i}\right]+G_k+G_b-\rho\varepsilon, \tag{4}$$

$$\frac{\partial}{\partial x_i}(\rho u_i c_p T)=\frac{\partial}{\partial x_i}\left[\alpha_T\left(\mu_{eff}\frac{\partial T}{\partial x_i}\right)\right]+\frac{\partial u_i}{\partial x_j}\left[\mu_{eff}\left(\frac{\partial u_i}{\partial x_j}+\frac{\partial u_j}{\partial x_i}\right)-\frac{2}{3}\mu_{eff}\frac{\partial u_k}{\partial x_k}\right]. \tag{5}$$

In Eqs. (1)–(5), subscripts $i, j, k = 1, 2, 3$ correspond to coordinates x, y, z; $C_{1\varepsilon} = 1.44$, $C_2 = 1.9$, $\sigma_k = 1.0$, $\sigma_\varepsilon = 1.2$, while μ_t, C_μ, G_k, G_b and other parameters used in the calculation can be found elsewhere [1]. Heat transfer coefficient and the Reynolds number are derived via Eqs. (6) and (7), respectively:

$$h=\frac{q}{t_w-t_f}, \tag{6}$$

$$\mathrm{Re}=\frac{ul}{v}. \tag{7}$$

Here q is heat flux density, t_w and t_f are the wall and fluid temperatures, respectively, u is fluid velocity, l is chord length, and v is viscosity coefficient.

2. **Study on Heat Transfer Coefficient**.

2.1. ***Heat Transfer Coefficient and Turbine Blade Cooling Relationship***. In the gas turbine, the heat transfer coefficient of the blade is very high, while the material thermal conductivity is quite low. This combination implies a specific distribution of the heat transfer coefficient along the entire blade, which is controlled by a low thermal conductivity.

A typical heat transfer coefficient distribution along the blade profile is depicted in Fig. 1. The heat transfer coefficient of the stagnation point (where the flow velocity is zero) is the largest and affected by the inlet turbulence, while the boundary layers at suction and pressure surfaces of the blade are turbulent or nearly turbulent. At the pressure surface of the blade, the laminar boundary layer is developed in the leading edge, but due to the influence of the incoming turbulence, the heat transfer coefficient gets higher than that in the front laminar flow. After that, the boundary layer changes successively and forms turbulent flows. The reason for the transformation is that the pressure gradient forces the boundary layer to keep the laminar flow state, while the blade curvature characteristics are more favorable for a turbulent flow.

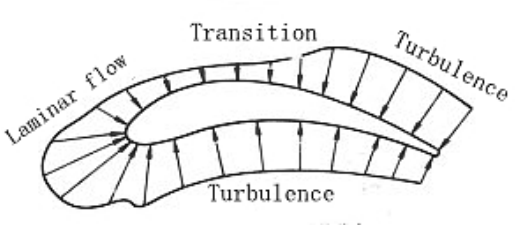

Fig. 1. A typical heat transfer coefficient distribution along the blade profile.

The distribution of heat transfer coefficient along the blade profile was calculated, in this study, by using the two-dimensional boundary layer theory. Firstly, the pressure distribution in the cascade was assessed by the numerical simulation of non-stick compressible two-dimensional flow. Then, the boundary layer was simulated using the boundary layer theory. The heat transfer coefficient distributions for different pressure values were found to be close to that depicted in Fig. 1. Although the calculated heat transfer coefficient distribution exhibited some singularities in the vicinity of the stagnation point and the suction layer laminar flow area, it proved to be quite accurate and robust. The heat transfer coefficient in the transition area (upper left part of Fig. 1) increased by 1.2~1.8 times due to the turbulence flow influence.

2.2. ***Preprocessing***. The turbine cascade model is depicted in Fig. 2, and its dimensions are listed in Table 1. As seen in Fig. 2, the high-temperature gas enters from the left (inlet) channel and flows out from the right (outlet) channel, the entrance angle of the cascade is 63.4°, the outlet angle is 28.4°, and the chord length is 43.942 mm.

The turbine cascade model meshing was implemented using the GAMBIT software for the pressure and suction walls (Fig. 3a and 3b) and inlet/outlet channels (Fig. 4a and 4b), respectively.

T a b l e 1

Turbine Cascade Model Dimensions

Chord length (mm)	Inlet channel inclination angle (deg)	Outlet channel inclination angle (deg)	Pitch (mm)
43.942	63.4	28.4	37.3

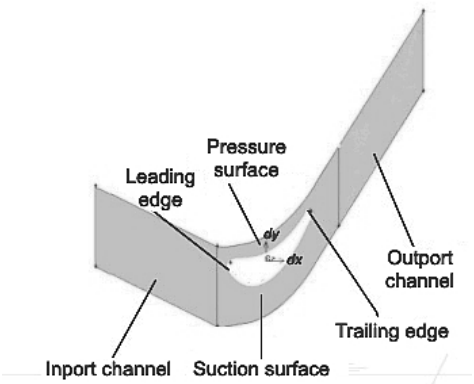

Fig. 2. Turbine cascade geometric model.

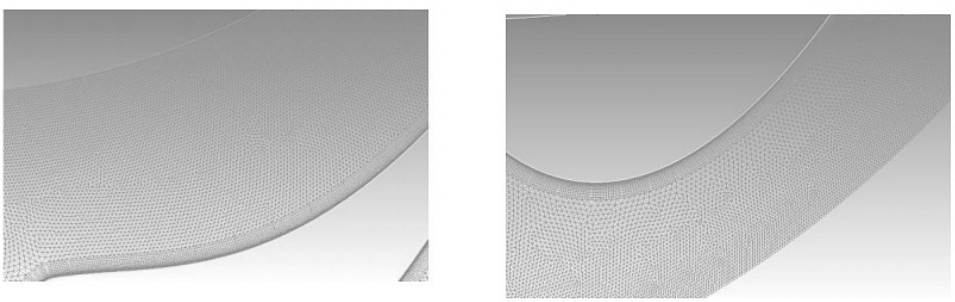

a b

Fig. 3. Pressure (a) and suction (b) surface wall grids.

T a b l e 2

Boundary Conditions

PR	Inlet pressure (MPa)	Outlet pressure (MPa)	Inlet/outlet temperature (K)	Blade wall temperature (K)	Temperature ratio
1.6	162.120	101.325	310	248	0.8
1.8	182.385	101.325	310	248	0.8
2.0	202.650	101.325	310	248	0.8

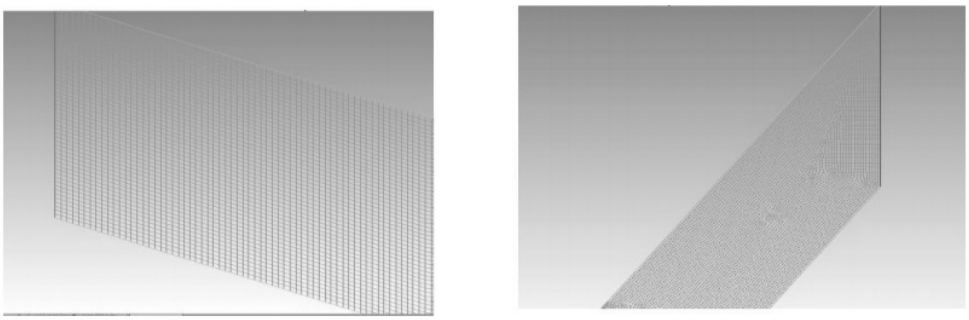

a b

Fig. 4. Inlet (a) and outlet (b) channel grids.

The boundary conditions are listed in Table 2, where three inlet/outlet pressure ratios (PR), namely 1.6, 1.8, and 2.0, are used, while the inlet/outlet temperature ratio is equal to 0.8.

2.3. ***Post-Processing***.

2.3.1. *Analysis of Heat Transfer Coefficient Distribution at Different Pressure Ratios*. For the pressure ratios of 1.6, 1.8, and 2.0 tabulated in Table 2, the heat transfer coefficient (HTC) values calculated at the same blade contour points exhibited an increase with the pressure ratio, which trend is illustrated by Fig. 5. The overall heat transfer coefficient distribution range is 200 to 1400 W/($m^2 \cdot K$). The convective heat transfer coefficient of the blade leading edge is the largest (1400 W/($m^2 \cdot K$), while that of the trailing edge exhibits a sharp increase (up to 1050 W/($m^2 \cdot K$), as is seen in Fig. 6.

2.3.2. *Analysis of the HTC Distribution along the Blade Profile*. The preliminary analysis shows that higher pressure ratios (and, thus, higher gas flow velocities) correspond to thinner boundary layers near the blade (and, thus, smaller heat transfer heat resistance). This complies with the well-known dependence $h = 1/(AR)$, where h is heat transfer coefficient, R is heat transfer resistance, and A is heat transfer area. If, under certain conditions, heat transfer resistance decreases in the constant heat transfer area, the heat transfer coefficient becomes larger.

2.3.3. *Analysis of the HTC Distribution at the Blade Leading Edge*. Firstly, a boundary (interface) layer is produced by the contact between the cooling fluid and the blade wall. This boundary layer is conventionally subdivided into the velocity boundary layer and thermal (temperature) one. The former one is defined as a thin layer, where the fluid velocity changes drastically near the solid surface. Its thickness corresponds to that where the velocity is 99% of the main velocity. The latter, i.e., thermal boundary layer, is defined as thin layer of fluid, with temperature changing drastically near the solid surface. There is a temperature difference between the mainstream and the wall under the condition

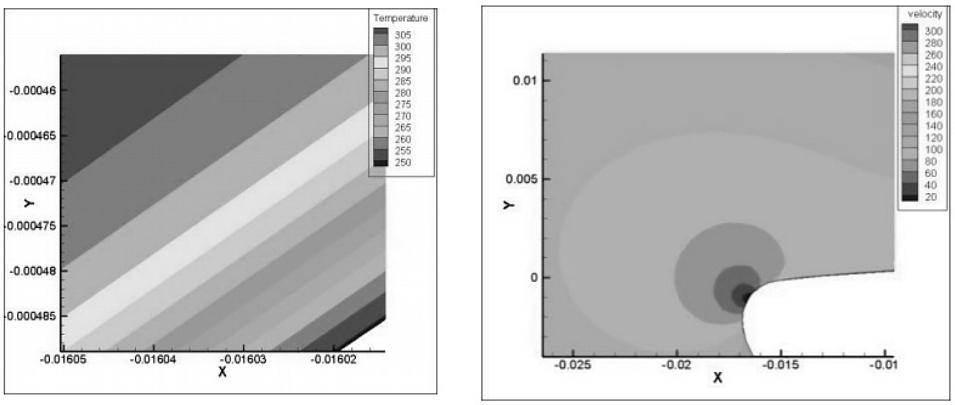

a b

Fig. 5. The calculated temperature (a) and velocity (b) distributions in the blade leading edge surface layer for pressure ratio $PR = 1.8$.

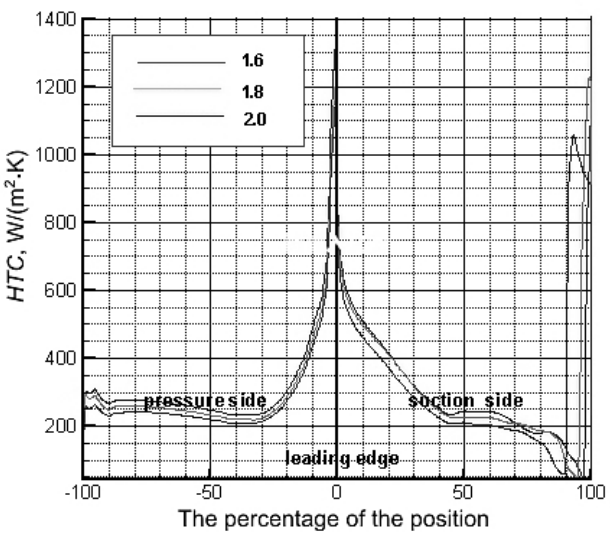

Fig. 6. Heat transfer coefficient curves for three *PR* values (1.6, 1.8, and 2.0).

of convective heat transfer. When the residual temperature at some distance from the wall equals to 99% of the mainstream excess temperature, the respective distance is referred to as the temperature boundary layer thickness. The heat transfer coefficient is related to the velocity and temperature boundary layer by the following relationship: $h = -\frac{\lambda}{\Delta t}\frac{\partial t}{y \partial y} = 1$.

When the temperature gradient in the temperature boundary layer is large, the convective heat transfer coefficient in the wall vicinity is also increased. Meanwhile, the velocity boundary layer also controls the convective heat transfer coefficient: when the cooling fluid velocity is relatively high, the impact of the fluid on the boundary layer is quite strong, so that the velocity boundary layer will be thinner, and the heat transfer resistance related to the latter will be quite small.

It can be seen from Fig. 6 that the heat transfer coefficient is the largest at the leading edge when the pressure ratio is 1.8, while Fig. 7 vividly illustrate that the temperature gradient of the leading edge is very large, but the velocity is very low (20~60 m/s).

T a b l e 3

The Heat Transfer Coefficient of the Leading Edge

PR	*HTC* of the leading edge [W/(m^2 · K)]	Increase rate (%)
1.6	1128.040	0
1.8	1186.216	5.157
2.0	1274.921	7.478

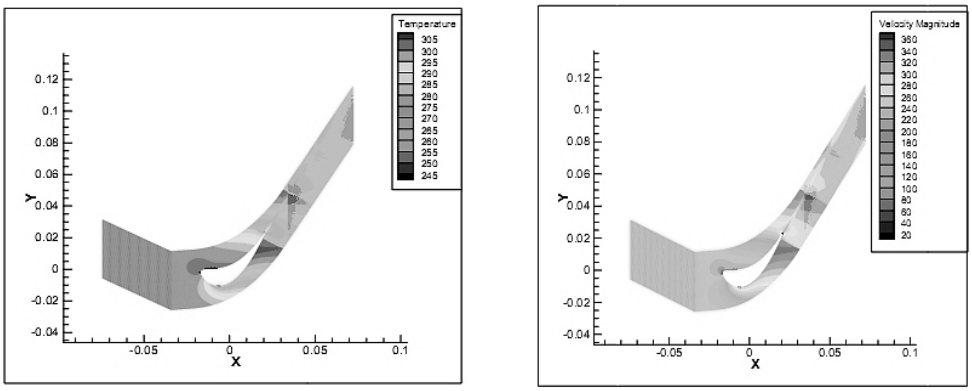

a b

Fig. 7. The calculated temperature (a) and velocity (b) distributions in the turbine cascade for pressure ratio $PR = 1.8$.

Therefore, according to the above findings, a high temperature gradient increases the heat transfer coefficient. While the leading edge flow velocity is low, the boundary layer thickness is high, and the convective heat transfer resistance is very large. So when the heat flux is constant, the convective heat transfer effect is relatively small: its values calculated at the blade leading edge for three different pressure ratios are shown in Table 3. When the *PR* changes from 1.6 to 1.8, the convective heat transfer coefficient increases by 5.157%, and when $PR = 2.0$, *HTC* increases by 7.478%, as compared to that at $PR = 1.8$. Therefore, the heat transfer efficiency of the turbine cascade is the lowest at $PR = 1.6$, and the highest at $PR = 2.0$. In other words, the heat transfer effect of the turbine cascade increases with the pressure ratio, while the convective heat transfer coefficient of the blade leading edge is the largest.

2.3.4. *Analysis of the HTC Distribution at the Pressure Edge*. The graph in Fig. 8 corresponds to three points of the pressure surface from the leading edge to the trailing one, which are the leading point, midpoint, and trailing point of the blade pressure surface. It can be seen from Fig. 9a that the temperature of the leading edge varies from 250 to 305 K, while the temperature boundary layer thickness is roughly equal to 0.000032 m. Consider the temperature gradient definition:

$$\frac{dt}{dx} = \frac{T_\infty - T_w}{\delta}, \tag{8}$$

where T_∞ and T_w are the temperatures of the mainstream fluid and the blade wall, respectively, while δ is the thermal boundary layer thickness. So the temperature gradient is $\Delta t/\delta = 1718{,}750$ K/m. From Fig. 9b, we can see that the temperature of the middle point is distributed (from 250 to 300 K), and the temperature boundary layer is approximately

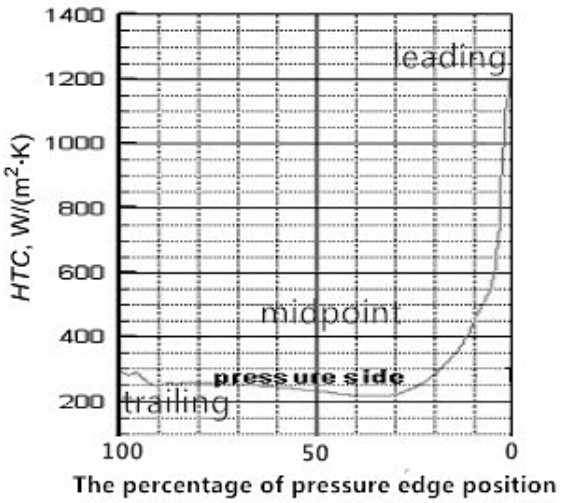

Fig. 8. Heat transfer coefficient distribution along the blade pressure surface.

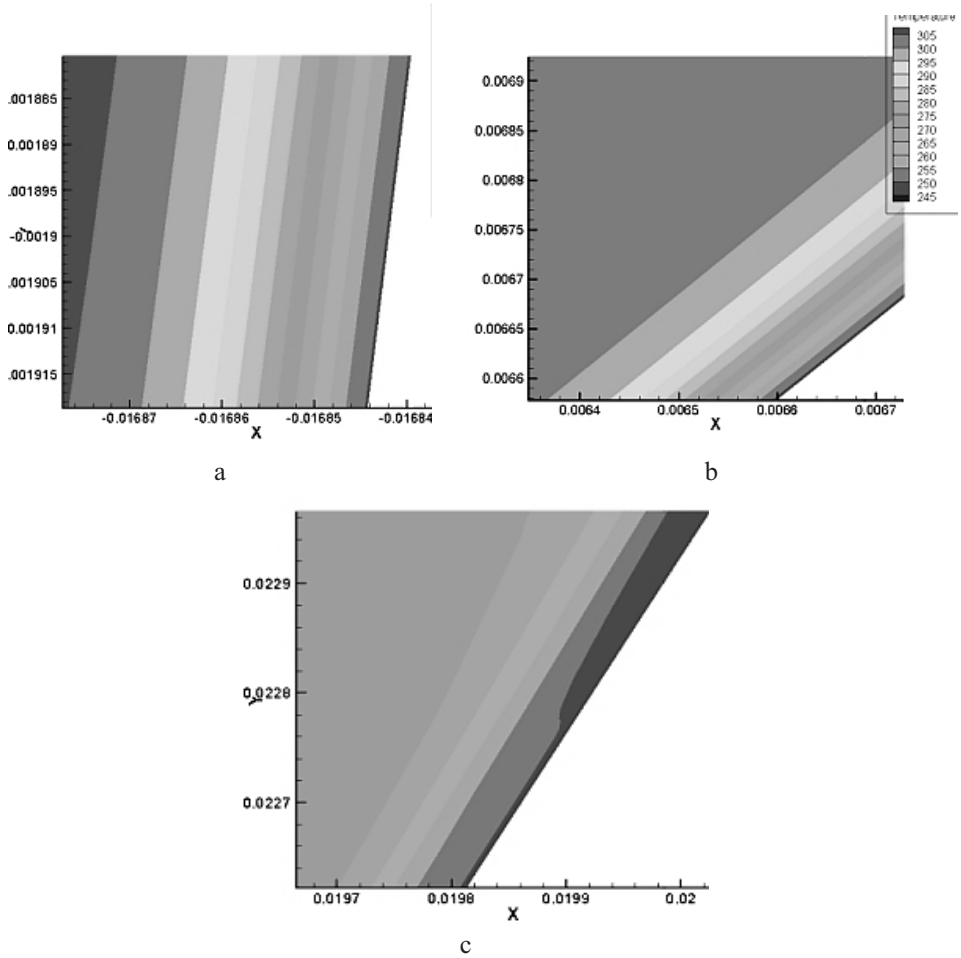

Fig. 9. Temperature distribution in the leading edge (a), midsection (b), and trailing edge (c) boundary layers of the turbine blade.

0.00024 m, so $\Delta t/\delta = 208{,}333.33$ K/m. As it follows from Fig. 9c, at the temperature boundary layer thickness is approximately equal to 0.00011 m, while and the trailing edge temperature varies by 25 K (from 250 to 275 K), so that $\Delta t/\delta = 227{,}272.72$ K/m. It can be seen that the temperature gradient varies from the leading edge to the trailing one on the pressure surface as follows: 1718,750, 208,333.33, and 227,272.72 K/m. This explains why the convective heat transfer coefficient is almost the same, except for a sharp drop from the leading edge to the trailing one.

2.3.5. *Analysis of the HTC Variation along the Suction Edge*. The heat transfer coefficient gradually decreases from the leading edge, and then increases quite abruptly when it reaches point *A*, as is shown in Fig. 10.

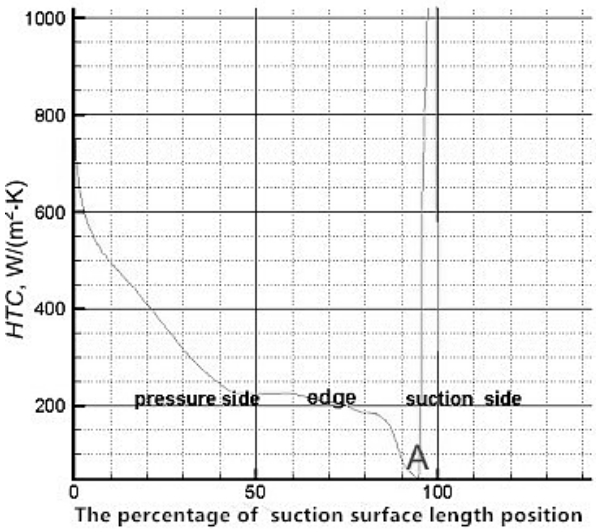

Fig. 10. Heat transfer coefficient distribution along the blade suction surface at $PR = 1.8$.

It can be seen from Fig. 11a that the temperature at the leading edge of the suction surface varies by 55 K (from 250 to 305 K), while the temperature boundary layer thickness δ is approx. 0.00005 m, so that $\Delta t/\delta = 1100{,}000$ K/m. Figure 11b indicates that the temperature boundary layer is approximately 0.00002 m-thick, while the temperature of the trailing edge varies by 10 K (from 250 to 260 K), so that $\Delta t/\delta = 500{,}000$ K/m. As seen from Fig. 12a, the temperature of the leading edge of the suction surface is about 250 K, and δ is approx. 0.00015 m, so $\Delta t/\delta = 0$ K/m. From Fig. 12b, it follows that δ is approx. 0.00003 m, and the trailing edge temperature varies by 30 K (from 250 to 280 K), so that $\Delta t/\delta = 1000{,}000$ K/m.

It is known that the temperature gradient evolution along the suction surface varies from 1100,000 to 500,000 K/m at the leading edge to 0–1000,000 K/m at the trailing one. This explains why the convective heat transfer coefficient from the leading edge to the trailing edge is reduced at first, and drops to zero and finally exhibits a sharp increase.

From Fig. 13, it can be seen that the gradient of the temperature boundary layer gradually drops from the leading point to point A, which results in a gradual drop of the heat transfer coefficient. The boundary layer separation occurs when point A is reached, so that the disturbance near the boundary layer becomes stronger, and the nearby laminar flow changes to a turbulent one. Meanwhile, the Reynolds number also increases, while the convective heat transfer resistance is small, making the convection thermal coefficient larger and, thus, strongly enhancing the heat transfer.

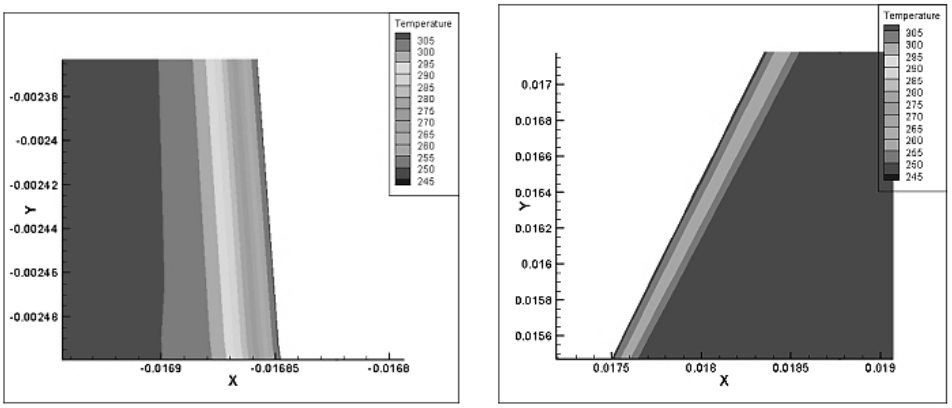

a b

Fig. 11. Temperature distribution in the leading edge (a) and midsection (b) blade suction surface at $PR = 1.8$.

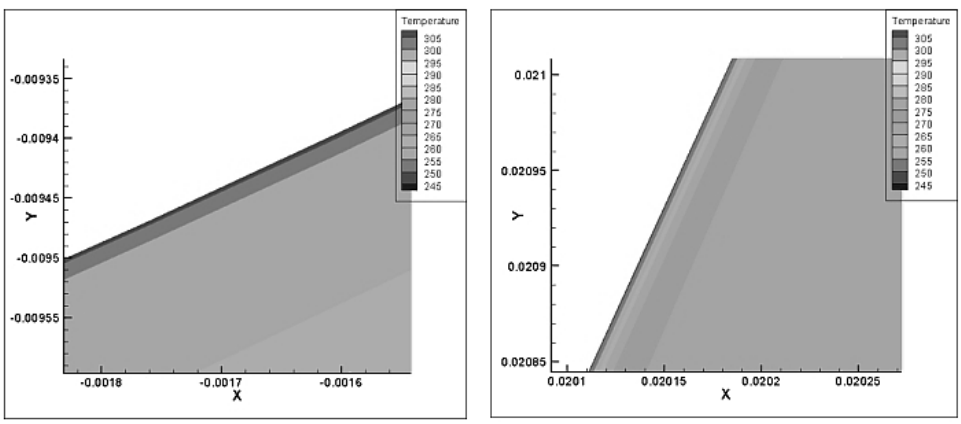

a b

Fig. 12. Temperature distribution in point A (a) and the trailing edge (b) of the blade suction surface at $PR = 1.8$.

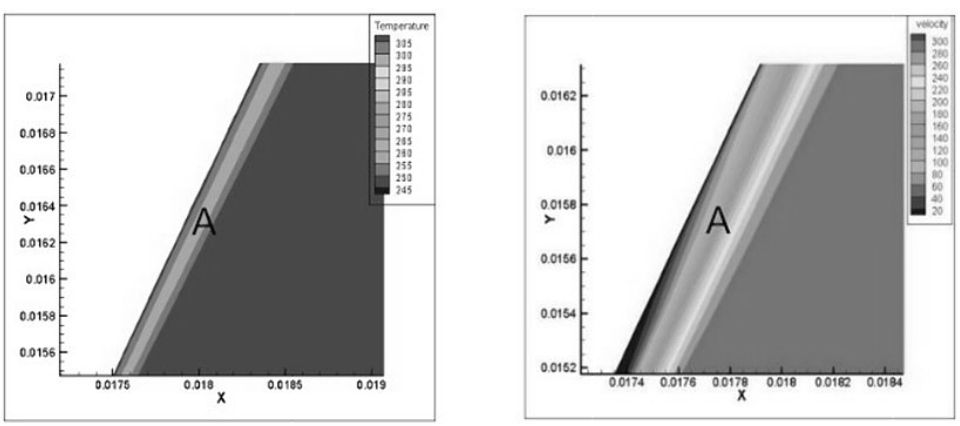

a b

Fig. 13. Temperature (a) and velocity (b) distributions calculated in point A of the blade profile.

Conclusions. In this paper, the effect of inlet/outlet pressure ratio on the heat transfer of the turbine cascade was explored, which made it possible to draw the conclusions:

1. For the examined pressure ratios of 1.6, 1.8, and 2.0, the heat transfer coefficient was found to increase with the pressure ratio at the same point of the blade profile. At the blade front, a change in the pressure ratio from 1.6 to 1.8 resulted in the convective heat transfer coefficient increase by 5.16%, and when the pressure ratio was raised to 2.0, the heat transfer coefficient increased by 7.48%, as compared to that at pressure ratio of 1.8. Therefore, the heat transfer efficiency of the turbine cascade is the lowest when the pressure ratio is 1.6 and the highest when the pressure ratio is 2.0. The overall heat transfer coefficient variation range was from 200 to 1400 $W/(m^2 \cdot K)$.

2. The heat transfer coefficient attained its maximum value at the blade leading edge and deceased along the pressure surface decreases from the leading edge to the trailing one. The heat transfer coefficient of the suction surface decreased from the leading edge to the trailing edge and exhibited a sharp rise at the tail point.

3. It was found that the three pressure ratios under study corresponded to different thickness values of the temperature boundary layer: larger pressure ratios invoked higher fluid velocities, thinner temperature boundary layers, and higher convective heat transfer coefficients.

Acknowledgments. This work was supported by the National Natural Science Foundation of China (No. 11602066) and the National Science Foundation of Heilongjiang Province of China (QC2015058 and 42400621-1-15047).

1. *Aeroengine Components, Aerodynamics, and Thermodynamics*, Aviation Industry Press (2016).
2. P. G. Hill and C. R. Peterson, *Mechanics and Thermodynamics of Propulsion*, Addison-Wesley (1965), pp. 5–32.
3. P. Kalghatgi and S. Acharya, "Improved film cooling effectiveness with a round film cooling hole embedded in a contoured crater," *J. Turbomach.*, **137**, No. 10, 101006, Paper No: TURBO-14-1279 (2015), doi: 10.1115/1.4030395.
4. R. S. Bunker, "Film cooling effectiveness due to discrete holes within a transverse surface slot," in: *ASME Turbo Expo 2002: Power for Land, Sea, and Air* (June 3–6, 2002, Amsterdam, The Netherlands), Vol. 3, Paper No. GT2002-30178, pp. 129–138 (2002), DOI: 10.1115/GT2002-30178.
5. G. Li, C. Wu, W. Zhang, et al., "Effect of cross-flow direction of coolant on film cooling effectiveness with one inlet and double outlet hole injection," *Propuls. Power Res.*, **1**, No. 1, 71–77 (2012).
6. D. A. Nealy, M. S. Mihelc, L. D. Hylton, and H. J. Gladden, "Measurements of heat transfer distribution over the surfaces of highly loaded turbine nozzle guide vanes," *J. Eng. Gas Turbines Power*, **106**, No. 1, 149–158 (1984).
7. J. Xu, J. Yao, J. Ja, et al., "Experimental investigation on the near-field character of film cooling with 30 deg injection from a row of holes on a convex surface," *J. Eng. Thermophys.*, **5**, 182–186 (1984).
8. Y. Liu, J. Huang, B. Yang, et al., "Duality of the interfacial thermal conductance in graphene-based nanocomposites," *Carbon*, **75**, 169–177 (2014).
9. F. Cao, Y. Liu, J. Xu, et al., "Probing nanoscale thermal transport in surfactant solutions," *Sci. Rep.*, **5**, 16040 (2015), doi: 10.1038/srep16040.
10. F. R. Menter, "Two-equation eddy-viscosity turbulence models for engineering applications," *AIAA J.*, **32**, No. 8, 1598–1605 (1994).

Received 05. 03. 2018